



Enhanced Growth of Green Synthesized $\text{Bi}_2\text{Fe}_4\text{O}_9$: Nanoparticles Decorated on MWCNT

A. AFROOS BANU¹, N. N. SHAFEEERA², N. KALANGADAN³, K. MOHAMED RAFI⁴,
D. SARAVANAKKUMAR⁵, K. RAJARAM⁶, S. A. FOWZIYA⁷, S. BEER MOHAMED⁸
and A. AYESHAMARIAM^{9*}

^{1,7}Department of Chemistry, Khadir Mohideen College, Adirampattinam, 614701

(Affiliated to Bharathidasan University, Tiruchirappalli), India.

^{3,6}Department of Microbiology, Central University of Tamil Nadu, Thiruvarur, 610 001, India.

⁴Department of Botany, Jamal Mohamed College (Auto), (Affiliated to Bharathidasan University, Tiruchirappalli), 620 020, India.

⁵PG & Research Department of Physics, Thiagarajar College, Madurai 625009, Tamilnadu, India.

⁸Department of Material Science School of Technology, Central University of Tamil Nadu, Thiruvarur, 610 001, India.

^{2,9}PG & Research Department of Physics, Khadir Mohideen College, Adirampattinam (Affiliated to Bharathidasan University, Tiruchirappalli), 614701, India.

*Corresponding author E-mail: ayeshamariamkmc@gmail.com

<http://dx.doi.org/10.13005/ojc/400103>

(Received: December 11, 2023; Accepted: January 21, 2024)

ABSTRACT

Bismuth ferrite nanoparticles decorated with multi-walled carbon nanotube nanoparticles were prepared using a Sol-Gel soft chemical approach technique. The synthesis was carried out under green conditions using high-quality acetate precursor salts. The carbon nanotubes were obtained from the germination of chippikalan oyster mushroom. The successful synthesis of the nanoparticles was confirmed by several characterization techniques, including structural, morphological, and optical studies. The nanoparticles were capped with various phytochemicals found in the leaf extract of *Murraya koenigii* and *Azadirachta indica*. The objective of the study was to evaluate the impact of biogenic Bismuth ferrite oxide multiwalled carbon nanotube nanoparticles on the growth of oyster mushrooms. The plant growth parameters such as stem length, breadth, germination spores percentage, spores germination rate, and mean daily germination were observed.

Keywords: Green synthesis, Bismuth doped Iron oxide MWCNT Nanoparticles, Pleurotus ostreatus oyster mushroom spores germination, *Murraya koenigii*, *Azadirachta indica*, antimicrobial activity.

INTRODUCTION

Bismuth has been a successful antibacterial

agent and aid in treating infections for the past ten years. The antibacterial effect of bismuth colloids is important for the treatment of peptic ulcers and

infectious diarrhoea (e.g., *Helicobacter pylori*). Bismuth subsalicylate's salicylate component may have anti-inflammatory and antisecretory effects on the intestines. It is amazing that Bi, a heavy metal that is fairly eco-friendly, has been used in photocatalysis, rubber production, energy storage, and pharmaceutical and medicinal applications. Pharmaceuticals, atomic fire alarms, and sprinkler systems, solders and other alloys, and pigments for cosmetics, glass, and ceramics are among the principal applications for bismuth. It also serves as a catalyst in the manufacturing of rubber¹.

The following features, such as capping agent, solvent medium choice, zero toxic material for NPs standardization, non-toxic material for nanoparticle stabilization, and effective size-reducing functional group candidate, are the main reasons why biosynthesis, along with green chemical roots, and eco-friendly perspectives of nanoparticle synthesis, are preferred²⁻³. The phytochemical structure functional groups, such as hydroxyl, methyl, carbonyl, carboxyl, amino, phosphate, and sulfhydryl groups compounds present in the leaf extracts that act as reducing and stabilizing agents, play a major role in the Bottom-Up green synthesis of nanoparticles using plant extract⁴.

Due to their benefits, such as being abundant in nature, cheap, and non-pathogenic, herbs and herbal parts are regarded as supporting agents for the synthesis of NPs. The process of creating nanoparticles from different biological sources, such as bacteria, fungi, yeast, chicken faeces, photosynthetic cyanobacteria, unicellular filamentous bacteria, agricultural waste, and home vegetable waste, is known as bio-synthesis⁵.

Mullite $\text{Bi}_2\text{Fe}_4\text{O}_9$ is a significant pharmaceutical nanoparticle that is used in a variety of environmental applications, including photocatalysis, water disinfection, air and water purification, organic forms, and the proliferation of plants. It also possesses properties like magnetics, electrical, electronic, and catalysis. These properties make it useful in fields like magnetoelectricity, multiferroics, optoelectronics, neuromuscular electrical stimulation (NMES), and microelectromechanical systems,(MEMS) Mico Electro Mechanical Systems spintronics, food and beverage processing, pharmaceuticals, and

antimicrobial applications. BFOMCNT is thought to be an excellent photocatalytic option for the photodegradation of dye compounds that have been promoted to indivisible complex molecules because it possesses a high degree of oxidizing property⁶. Nanoparticles are used in the environment for a variety of magnetic, photocatalytic, and dielectric investigations as well as medical applications. For the creation of natural nano manures and nano insect stoppers, plant cultivation organic farming areas use nanoparticles such as bismuth, Iron, copper, silver, and gold. These materials also promote the growth of leaves and improve leaf germination and plant growth⁷.

Curry leaves are typically used in all spicy south Indian cuisines to enhance the flavour, aroma, and for nutritional benefits. The Neem leaves are to be consumed raw for killing are present in the intestine and utilized as a disinfecting agents in home cleaning. Both leaves have high antioxidant properties and are frequently employed as a capping agent in key green synthesis of NPs. These leaves are also used in toothpastes, anti-inflammatory lotions, and external antiseptic medications⁸⁻¹⁰. In the past, the extract of BFOMCNT NPs has been utilized to synthesize metal oxide nanoparticles such Ag, Fe, Cu, and Au¹¹. Copper and silver nanoparticles made from *Murraya koenigii* and *Azadirachta indica* were used in antimicrobial studies¹².

According to previous reports, 100 g of curry leaves contain bioactive compounds such as flavonoids ($7.43 \pm 0.03\%$), phenols ($4.25 \pm 0.04\%$), saponins ($2.50 \pm 0.01\%$), alkaloids ($1.90 \pm 0.01\%$), tannins ($0.86 \pm 0.02\%$), and glycosides ($0.11 \pm 0.01\%$). According to the analysis, the proximate composition is as follows: carbohydrate content is $39.44 \pm 0.04\%$, moisture content is $23.42 \pm 0.10\%$, crude fibre is $6.30 \pm 0.05\%$, ash content is $15.60 \pm 0.21\%$, lipids are $6.48 \pm 0.22\%$, and protein is $8.38 \pm 0.02\%$. Vitamin A (beta-carotene) was present at 6.04 ± 0.02 mg/100 g, vitamin C (ascorbic acid) at 0.04 ± 0.002 mg/100g, thiamin was present at 0.89 ± 0.01 mg/100g, riboflavin was present at 0.09 ± 0.001 mg/100 g, niacin was present at 2.73 ± 0.02 mg/100 g, and vitamin E was present at 0.03 . The plant leaf was discovered to contain certain significant minerals, including calcium (19.75 mg/100 g), magnesium (49.06 ± 0.02), sodium (16.50 ± 0.21 mg/100 g), potassium (0.04 ± 0.001 mg/100 g), and zinc

(0.04–0.001 mg/100 g)¹³. In order to promote its usage as a medicinal plant and as a food flavouring and spicing condiment, the leaves of the curry plant contain a significant number of essential phytochemicals that have antioxidant capabilities as well as some nutritional vitamins and minerals¹⁴. A fresh leaf of *A. indica* yields a maximum of 59.4% moisture, 22.9% carbs, 7.1% proteins, 6.2% fibre, 3.4% minerals, and 1% lipids and other compounds per 100 g of its nutritional value¹⁵.

As of our knowledge, till date there hasn't been any information published on the green synthesis of BFOMCNT NPs utilizing *Murrayakoenigii* and *Azadirachta indica* leaf extract. Additionally, this is the first study to use *Murrayakoenigii* and *Azadirachta indica* green synthesised BFOMCNT NPs¹⁶.

It has been laudably demonstrated that iron metal oxides (IMOs) with nanostructures work as a germination inducer and the leaves exposed to CNTs are observed to increase the germination and growth rate of vegetable plant leaves. The leaves in the control experiment (without CNTs) did not germinate in the same amount of time as the leaves placed in the MS medium with the various concentrations of CNTs. In addition to having more biomass than control plants, vegetable plants grown in media enriched with CNTs also had well-developed long stems¹⁷.

The use of BFOMCNT NPs in the investigation of mushroom spore germination is the main emphasis of the current study. Although BFOMCNT NPs were biosynthesized from plant extract, a mushroom growth test was conducted in vivo condition to evaluate the effects of biosynthesized BFOMCNT NPs on plants¹⁸. In India, neem trees and *Murrayakoenigii* (iron-rich green leaves) are both known as curry leaves Figure 1.



Fig. 1. Germination assay In vivo effect of BFOMCNT NPs on growth of oyster mushroom (*Pleurotus ostreatus*) spores

EXPERIMENTAL

MATERIALS AND METHODS

All chemical salts, including the precursor to MWCNT Bismuth(III) and Ferrous(II) acetate (TTIP), were bought from Sigma-Aldrich. MWCNT liquid solution was prepared over the course of two days using ultrasonication, and all aqueous suspensions were appropriately made with double-distilled (DI) water. All of the reagents used were of analytical quality. The curry and neem leaves were harvested from their respective plants in the Adirampattinam region of Thanjavur district, Tamil Nadu, India¹⁹.

Synthesis of BFOMCNT NPs

Fresh, healthy leaves of *Murrayakoenigii* and *Azadirachta indica* were thoroughly washed multiple times with de-ionized water to eliminate the dust particles sticking on the surface before being used to prepare the leaf extract. The two leaves were then boiled separately for 20 min at 50 degrees in a beaker using a hot water bath. The extract was then put into a glass jar after being filtered via Whatman filter paper. 0.1 M solution of BFOMCNT in a separate beaker containing 100 mL was agitated for two hours in order to obtain BFOMCNT nanoparticles. A 100 mL of BFOMCNT solution was agitated at room temperature for 24 h with 20.0 mL of *Murrayakoenigii*'s aqueous leaf extract added (Sample 1). *Azadirachta indica*'s aqueous leaf extract was added in 20.0 mL increments to a 100 mL BFOMCNT solution, which was agitated for 24 h at room temperature (Sample 2). 20.0 mL of the aqueous leaf extract from each of the *Murrayakoenigii* and *Azadirachta indica* plants were added to 100 millilitres of the BFOMCNT solution and mixed for 24 h at room temperature (Sample 3). After being rinsed with ethanol and de-ionized water, the resulting BFOMCNT NPs were centrifuged at 6000 rpm for 15 min with double-distilled water. Precipitates were then collected, dispersed, and filtered. Then, the cleaned BFOMCNT NPs are placed on a petri dish and heated for a one hour at 40°C in a hot air oven. The obtained nanoparticles were ground in a granite mortar and pestle before being employed for germination and analytical characterization.

Characterizations

Using an X-ray powder diffraction (XRD) PAN analytical X-ray diffractometer with CuK α radiation ($\lambda=1.5406 \text{ \AA}$), the crystalline phases of

the materials were studied in order to determine the green synthesis reduction of the Fe and Bi linked MWCNT in the samples. Using the UV-Vis-NIR spectrophotometer Hitachi 3400 was used to measure the UV-Vis absorption. The Fourier Transformation Infrared (FTIR) spectrometer in the transmittance mode in the region of 4000-400 cm⁻¹ was used to validate the functional group of the materials.

To isolate mushroom spores and keep them alive in a pure culture in test tubes or petri plates, a culture medium is necessary. The fungi can be grown on solid agar media or in liquid media (broths). (Agar agar is a material that solidifies when cooled and is made from seaweed like *Gelidium sp.*, which melts when heated.) The environment for germination was created in a very random, unclean, and well-ventilated location. To provide a clean surface and to prevent any insect disturbance, oyster mushroom (*Pleurotus ostreatus*) spores were submerged in an 800 mL NaCl solution for five minutes. They were then soaked in pure rainwater. For five hours, seeds were exposed to various concentrations of BFOMCNT NPs, as well as a control. *Pleurotus ostreatus* growth was assessed using the effects of three combinations of BFOMCNT NPs, 30 mL, and compared to untreated control spores.

Following the establishment of the culture of germination, spore germination was observed everyday for one week, and spores were deemed to have germinated when the petals were stretched to a length of more than 2 cm. Additionally, the number of petals was counted and data were recorded at the conclusion of the germination experiment. And the antimicrobial properties of the synthesized nanomaterial was assessed using a zone of inhibition studies as well as by minimum inhibition concentrations (MIC). Briefly, a 10 µL concentration of nanomaterials sample were spotted on the bacterial lawns of *Pseudomonas aeruginosa* (Gram-negative) and *Staphylococcus aureus* (Gram-positive), and the upon overnight incubation the inhibition zones were measured. To determine the MIC of each sample, overnight grown bacterial cultures were standardized to 0.5 McFarland standard to obtain a cell number of 1.5×10^8 cells/mL followed by a 200 µL of sterile Luria Bertani broth and 10 µL of test cultures

containing 1.5×10^6 cells/mL (*S. aureus* and *P. aeruginosa*) were added to the designated wells of 96 well plates, except for the positive control. And different dilutions of the sample were added to the designated well and incubated overnight (16 h) in the shaking incubator. The next day, MIC values were determined.

Hemolysis–Biocompatibility Assay

A 5 mL of blood was collected in an anti-coagulant (EDTA) containing tube and centrifuged at 1500 rpm for 10 min and the sedimented pellets containing red blood cells were taken and washed well with Phosphate Buffer Saline (PBS) buffer and diluted the Red Blood Cells (RBCs) with PBS buffer to the volume of 6 mL. From this, 100 µL of RBC samples were transferred to 2 mL microcentrifuge tubes. To one of the tubes containing RBC cells, a 500 µL of 20% Triton X was added and treated as a negative control while the same volume of PBS-added microcentrifuge tube was assumed as a positive control. The samples of nanoparticles containing BFOMCNT, BFOMCNT+curry, and BFOMCNT+curry+neem were added to the vials and incubated at least for 4 h at 37°C. After incubation, the vials are vortexed briefly and centrifuged at 5500 rpm for 15 min and the pellets discarded, and the (OD) oxygen demand of the supernatant gained was read at 575 nm using Bio-Rad iMark microtiter plate reader and the percentage of the hemolysis was analyzed.

Percentage of hemolysis = (sample absorbance-absorbance of PBS)/(absorbance of Triton X-absorbance of PBS) *100 (32).

RESULTS AND DISCUSSION

XRD Analysis

Figure 2 displays the powder X-ray diffraction (XRD) pattern of the synthesised BFOMCNT NPs obtained in the current investigation. Additionally, it supports the fact that biosynthesised BFOMCNT NPs are crystalline. The entire range of 2 values is accurately represented by six strong wide peaks in the XRD pattern. The notable diffraction peaks in Fig. 2 are indexed as (111), (121), (211), (211), (022), and (410) Miller indices values, which are located at 23.8, 28.06, 29.168, 34.023, 36.9525, 39.446 and 46.487 correspondingly. These findings concur with those in the JCPDS file No. 74-1098²⁰.

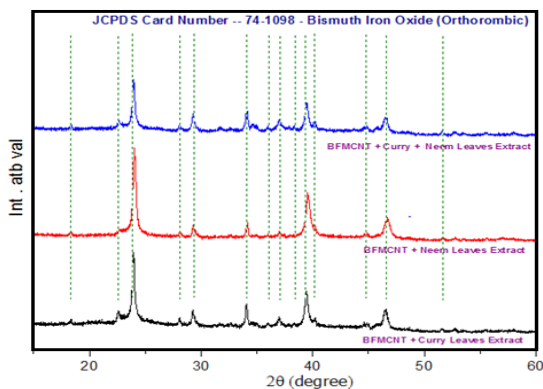


Fig. 2. X-ray diffractometer Analysis BFOMCNT NPs with Curry, Neem and Curry with Neem leaves extract

Table 1: Structural Analysis of (BFOMCNT NPs) +Curry Leaves Extract

2θ	θ	FWHM	$\frac{0.94\lambda}{\beta \cos\theta}$	$\frac{1}{D^2}$
23.885	11.9425	0.3615	40.901	0.000598
28.056	14.028	0.3764	39.650	0.000636
29.168	14.584	0.3971	37.691	0.000704
34.023	17.0115	0.2594	58.394	0.000293
36.952	18.476	0.3549	43.032	0.00054
39.446	19.723	0.3956	38.891	0.000661
44.735	22.3675	0.3428	45.690	0.000479
46.487	23.2435	0.4217	37.380	0.000716

Table 2: Structural Analysis of (BFOMCNT NPs)+Neem Leaves Extract

2θ	θ	FWHM	$\frac{0.94\lambda}{\beta \cos\theta}$	$\frac{1}{D^2}$
23.991	11.9955	0.3625	40.841	0.0006
27.956	13.978	0.3774	39.541	0.00064
29.968	14.984	0.3991	37.562	0.000709
34.523	17.2615	0.2694	56.290	0.000316
37.952	18.976	0.3449	44.400	0.000507
39.946	19.973	0.3256	47.323	0.000447
44.935	22.4675	0.3628	43.194	0.000536
46.887	23.4435	0.4317	36.311	0.000758

Table 3: Structural Analysis of (BFOMCNT NPs)+Curry+Neem Leaves Extract

2θ	θ	FWHM	$\frac{0.94\lambda}{\beta \cos\theta}$	$\frac{1}{D^2}$
24.093	12.0465	0.3665	40.403	0.00613
28.216	14.108	0.3794	39.957	0.000613
29.998	14.999	0.4001	37.471	0.000626
34.923	17.4615	0.2684	56.561	0.000712
38.152	19.076	0.3449	44.427	0.000313
40.146	20.073	0.3259	47.309	0.000507
45.135	22.5675	0.3528	44.451	0.000447
46.987	23.4935	0.4219	37.42	0.000506

FTIR Analysis

The FTIR spectra of the BFOMCNT NPs, which were made from a green leaf combination, were acquired from the transmittance IR peaks. According to the FT-IR study's findings, transmittance peaks were found at approximately 3022.01 cm⁻¹,

1659.53 cm⁻¹, 1311.26 cm⁻¹ and 566.52 cm⁻¹(Fig. 3). The functional group of BFOMCNT is observed at 3001.01 cm⁻¹ because of the presence of an aromatic functional group (C-H), 1613.94 cm⁻¹ because of the stretching of primary amines along the N-H axis, and 1310 cm⁻¹ because of the presence of alcohols, carboxylic acids, esters, and ethers along the C-O axis. Peak around 3000 cm⁻¹ was caused by the -OH stretching and C - C stretch, and the alkenes are shown between 1600 and 1652 cm⁻¹. The peaks seen at 566.52 cm⁻¹ for the green leaf extract are proof that BFOMCNT NPs were synthesized²¹.

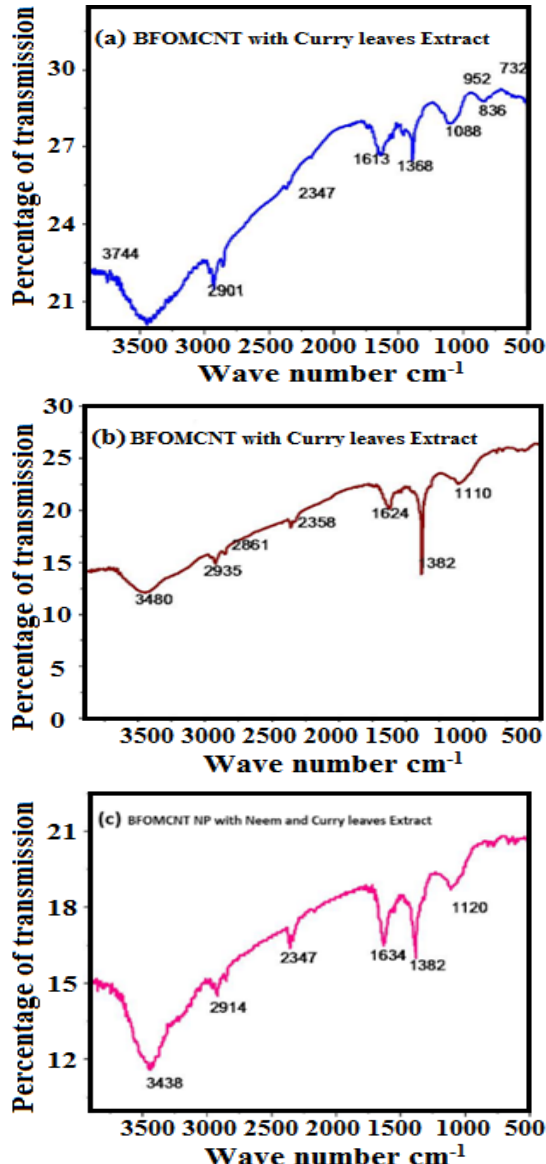


Fig. 3. FTIR Analysis of BFOMCNT NPs with Curry, Neem and Curry with Neem leaves extract

UV-Vis Studies

Figure 4 displays the examination of the BFOMCNT NPs with Curry, Neem, and Curry with Neem leaves extract in terms of absorbance, transmission, and bandgap. Fig. 4a and 4b demonstrate a linear increase in absorbance and transmission from sample 1 to Sample 3. Semiconductor materials exhibit the region where light absorption increases steeply and linearly as energy increases. An estimation of the band gap energy is provided at the x-axis intersection point of the Tauc plot's linear fit. Samples 2 and 3 have bandgap values of (4.31 eV, 4.14 eV and 3.88 eV) respectively²².

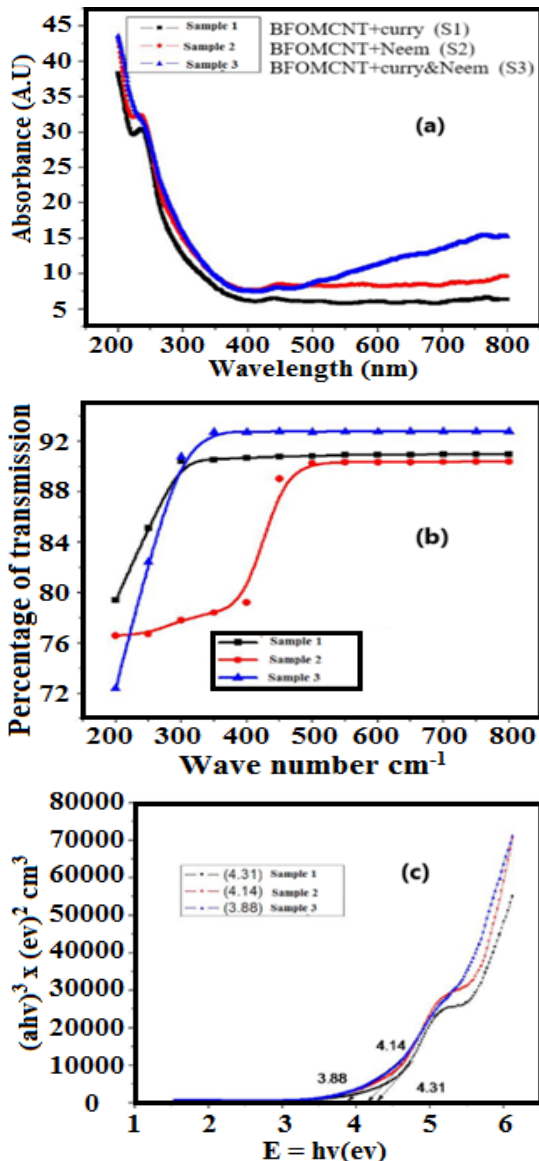


Fig. 4. UV-Absorbance, Transmission and Bandgap Analysis of BFOMCNT NPs with Curry, Neem and Curry with Neem leaves extract

The antibacterial study and its mechanism

Using the agar zone of inhibition study on Mueller-Hinton agar (MHA), the antibacterial effects of BFOMCNT, BFOMCNT+curry, and BFOMCNT+curry+neem extracts against *Gram-positive* (*Staphylococcus aureus*) and *Gram-negative* (*Pseudomonas aeruginosa*) bacteria were examined. The BFOMCNT and BFOMCNT+curry+neem were shown zone of inhibition while the BFOMCNT+curry leave extract did not show any visible clearance on the agar plate. The BFOMCNT+curry+neem has shown a larger zone, as it may be due to the synergistic mechanism of neem and curry leave extract. The MIC values for all three samples were analysed and the values were tabulated in Table 1. The MIC values for the two bacterial samples used follow this pattern BFOMCNT+curry leaves+neem leaves>BFOMCNT>BFOMCNT+curry leaves. The MIC value for the BFOMCNT for *S. aureus* and *P. aeruginosa* are 5 mg/mL and 4 mg/mL respectively. While for the BFOMCNT+curry leaves+neem leaves, it was 1 mg/mL and 0.5 mg/mL respectively. There was no inhibition of test bacteria has been observed for the BFOMCNT+curry leaves. It may be due to the reason, the curry leaf extracts mask the activity of the nanoparticles.

The hemotoxicity of the samples was analyzed and the percentage of hemolysis was given in Fig. 5(a-b). Triton X, a nonionic surfactant that is known for hemolysis is used as a positive control and the lysis observed while incubating with the triton X is considered 100% while the lysis observed with the PBS treatment is assumed as a negative control. All the three samples such as BFOMCNT, BFOMCNT+curry leaves, and BFOMCNT+Curry+Neem nanopowder has shown toxicity in the range between 6-7% that confirms the samples are biocompatible and can be applied for *in-vivo* and *in-vitro* studies and human applications (Mary AS et al., 2021).²³

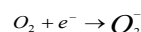
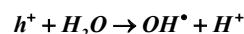
The antibacterial efficiency of BFOMCNT+Curry+Neem nanopowder is generally determined by the following three factors as follows:

- (a) Percentage of deliverance of reactive oxygen species (ROS),
- (b) Percentage of Bi^{2+} and Fe^{2+} ion and
- (c) Geometrical nature of particles and its volume

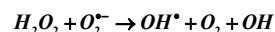
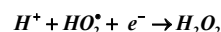
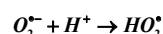
According to the fundamental ideas of electromagnetic waves, when green produced nanoparticles interact with a sufficient amount of light energy that roughly matches the value of the energy gap, A vacancy was created in the valence band (VB) as a result of an electron being electronically excited from a lower energy level to a higher energy level, such as from valence band (VB) to conduction band (CB), h^+ holes recombination, h^- electron recombination.

$\text{Bi}_2\text{Fe}_4\text{O}_9$; MWCNT+(Curry+Neem) leaves extracts+

In the environment of the interaction between the sample and the microbe, the electrons at higher energy levels (CB) as well as the holes created in the lower energy level (VB) cause the emanation of the following substances, including hydrogen peroxide, hydroxyl radical ions (HRI), reactive oxygen species (ROS), and super oxide anion (O_2^-)-(SOA).



The disruption of microbes by ROS led to the formation of the cell membrane's aperture as a result of the dissociation of the DNA, pilus, plasmid, ribosome, cytoplasm, cytoplasmic membrane, cell wall, capsule, nucleoid, and flagellum. This resulted in the bacteria being in an active state or completely broken up into numerous pieces. Additionally, when the holes contact with them, which are depicted as follows in a synchronous manner, BFOMCNT+Curry+Neem nanopowder, ROS are formed²⁵.



The following proposed mechanism is applicable for all samples. According to the Haber-Weiss reaction theory, certain ions and oxides participate in the initial stage of this interaction, where hydroxyl and hydroxide ions are produced from the reaction of H_2O_2 and superoxide ion catalysed by iron. Hydrogen peroxide is less toxic in nature than reactive oxygen species (ROS), but it exhibits aberrant dissociation when it interacts with bacterial biomaterials. As a result, when H_2O_2 interacts with SOA, OH^\bullet radicals are released. Additionally, in the BFOMCNT and other systems,

the formation of doubly ionised oxygen vacancies (DIOV), electromagnetic wave and photostimulated e generation, and conduction band electrons are provided free²⁶.

According to the notion of inherent crystalline point defects, DIOVs are created during the production of BFOMCNT regardless of the synthesis method used. Therefore, the number of flaws contributes to the frequency of oxygen empty spaces. This mechanism is supported by UV-Vis data, which show that the DIOVs have a significant absorption curve at around 200 nm. This curve is observed to be strong in the case of BFOMCNT+Curry+Neem nanopowder, with the exception of samples (a) and (b). When compared to other samples, the BFOMCNT+Curry+Neem nanopowder sample had a higher number of " O^- " vacancies. The increased production of oxygen vacancies in the nanocrystalline samples is thought to be caused by the direct correlation of phytochemicals with the release of simple ions into the BFOMCNT base²⁷.

The following are the effects of the liberation of the ions Bi^{2+} and Fe^{2+} in the samples: Free metal ions are released from the system as a result of the additional entry into the scene of phytochemically treated two samples' green molecules during photo electron generation that pushes the two transition metal ions Bi^{2+} and Fe^{2+} into the occupied spaces. More metal ions were released from the nanopowder as a result of this. The XRD crystallographic data, which clearly clarified the consideration of alternative association of the phytocompounds agrees with our proposed mechanism, and the strong observation of the UV-band and FTIR peaks at 200 nm and 462 nm, respectively, agree to the Bi and Fe observed for this sample. Due to the strong electrostatic interaction between the positively charged ions and the negatively charged cytoplasmic membrane of the bacteria, more Bi^{2+} and Fe^{2+} ions are released from the surface of the nanopowder, which causes the bacterium colony to vanish²⁸.

The S/V ratio and geometrical particles

The size and form of the particles play a significant role in the antibacterial properties of the nanoparticles being investigated. It is thought that the effective antibacterial activity of the samples in this work is clarified by the combination of

phyto-compounds from green herbs with metallic oxide NPs. The active spikes of the non-uniform surface that would cause strong electrostatic interaction between the cell wall and ion when electromagnetic photons impact on the samples in the ambient temperature are explained by the surface morphology photographs. The important thing to note, however, is that the nanopowders' corner edges execute the response rate of ions' emission by penetrating the cell wall, much as how puncturing a banana with a needle causes noticeable disruptions to the bacterial community as a whole. It has been noted that the double cationic nanopowder easily exhibits strong antibacterial action against both *Gram+* and *Gram-* microorganisms. The following factors are responsible for this finding according to the hypothesised mechanism: *Gram-positive* and *Gram-negative* bacteria have strong walls and several internal and external layers²⁹.

In general, antibacterial efficiency of a BFOMCNT+Curry+Neem nanopowder depends on three factors concentration generation ROS, percentage of releasing of Bi^{2+} and Fe^{2+} ions and geometrical structure of surface of nanopowder. The

BFOMCNT+Curry+Neem nanopowder created in the current work is discovered to demonstrate dominant influence over their untreated with herbal extracts in all three parameters. This is due to the double cationic Bi^{2+} and Fe^{2+} . A much larger concentration of ROS and interstitial double cationic species are released from the herbal treated samples, according to the structural and optical data of the values observed from the XRD and Bacteria tests. Fig. 6 clearly illustrates the hypothesised mechanism for the inhibitory steps of the double cationic BFOMCNT+Curry+Neem nanopowder. The spherical and nonuniform particles are seen in the surface morphology photos, which firmly support the aforementioned suggested actions³⁰.

Table 4: Represent the minimum inhibitory concentration (MIC) of the samples S1, S2, S3 for bacterial isolate *S. aureus* and *P. aeruginosa*

S. No	Samples	MIC values	
		<i>S. aureus</i>	<i>P. aeruginosa</i>
1	BFOMCNT	5 mg/mL	4 mg/mL
2	BFOMCNT+curry leaves	No inhibition	No inhibition
3	BFOMCNT+curry leaves +neem leaves	1 mg/mL	0.5 mg/mL

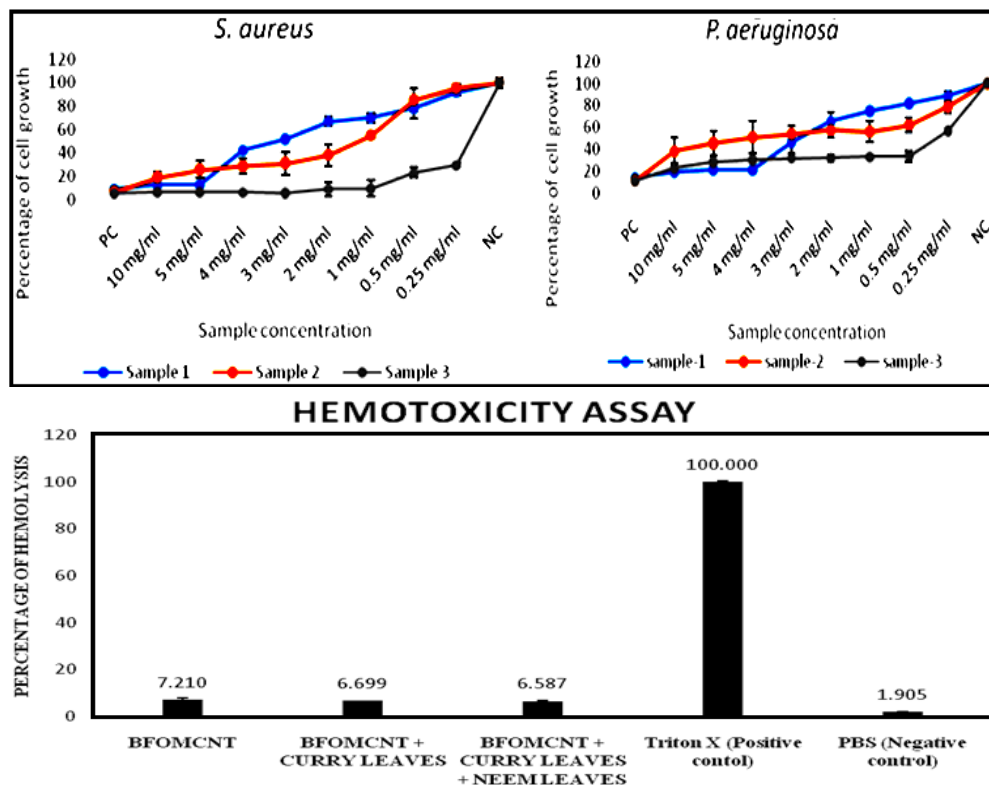


Fig. 5(a-b). Antibacterial and Hemotoxicity assay of BFOMCNT NPs with Curry, Neem and Curry with Neem leaves extract

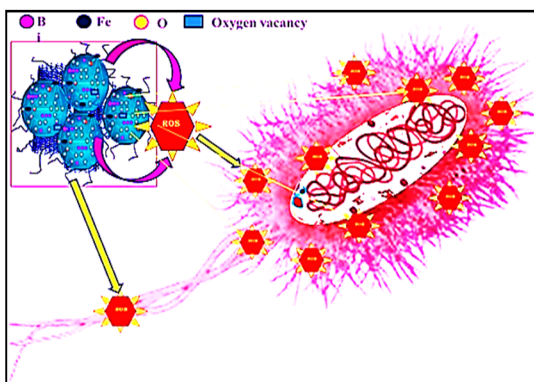


Fig. 6. Schematic representation of DIOV and ROS mechanism

As shown in Fig. 6, various germination characteristics for mushrooms, including germination%, rate, value, and mean daily germination, were examined. Varied quantities of BFOMCNT+Curry+Neem nanopowder caused different reactions in *Pleurotusostreatus* oyster spores. In spores treated with 30 g mL⁻¹ of BFOMCNT+Curry+Neem nanoparticles, spore germination of *Pleurotusostreatus* rose dramatically from 10% to 100%. The growth rate and germination potential of *Pleurotusostreatus* spores were improved when the double metal concentration was raised to particular amounts. However, the maximum BFOMCNT+Curry+Neem nanopowder concentration, 100 µg/mL, greatly increases *Pleurotusostreatus* mushroom spore germination. In comparison to lower concentrations, the iron nanoparticles promoted the development of *Pleurotusostreatus* spores in higher concentrations. When spores were exposed to nanoparticle concentrations ranging from 0 to 100 µg/mL, they germinated at a rate of about 100% as opposed to the untreated mushroom. The double cations with phyto-nutritional qualities are visible in the herbal-treated mushroom photos, which firmly confirm this

germination culture^{31,32}.

CONCLUSION

The green synthesis technique was used to successfully create BFOMCNT+Curry+Neem nanopowder from *Azadirachta indica* and *Murrayakoenigii* leaves. It was established that BFOMCNT is in its pure orthorhombic form and has the best shifts. BFOMCNT was converted to BFOMCNT nanoparticles by phytochemicals found in the leaves extract of *Murrayakoenigii* and *Azadirachta*. And these nanoparticles are biocompatible. The average crystalline size of the sample was determined to be 28.96 nm through the investigation of the structural studies by XRD. The multiplication of mushroom spores and mushroom germination both clearly demonstrate the mushroom's efficient growth. The outcomes show that BFOMCNT NPs have positive efficacy in curry and neem leaf extract-induced mushroom growth enhancement. The antibacterial effectiveness is improved as a result of the increase in spike area and the NPs' capacity to poke. The key candidate for both mushroom germination and antimicrobial operating systems, the BFOMCNT nanopowder's double cations have been used to improve the antibacterial properties.

ACKNOWLEDGMENT

The Department of Microbiology at the Central University of Tamil Nadu in Thiruvarur is gratefully acknowledged for approving and supporting this research.

Conflict of Interest

No conflict of interest is associated with this work.

REFERENCES

- Mathew, S.S.; Sunny, N.E.; Shanmugam, V. *Inorganic Chemistry Communications.*, **2021**, 126, 108485-108492.
- Huang, R.; Zhou, Z.; Lan, X.; Tang, F.K.; Cheng, T.; Sun, H.; Ken, K.C.; Li, L.X.; Jin, L. *Materials Today Bio.*, **2023**, 100507-100513.
- Voss, L.; Hsiao, I.L.; Ebisch, M.; Vidmar, J.; Dreick, N.; Böhmert, I.; Stock, V.; Braeuning, A.; Loeschner, K.; Laux, P.; Thünemann, A.F.; Lampen, A.; Sieg, H. *Food Chem.*, **2020**, 1-35.
- Hannachi, E.; Slimani, Y. *Handbook of Magnetic Hybrid Nanoalloys and their Nanocomposites.*, **2022**, 351–385.
- Campo, G.; Pineider, F.; Fantechi, E.; Innocenti, C.; Caneschi, A.; Fernández, C.J. *J Nanosci Nanotechnol.*, **2019**, 4946-4953.
- Mala, N.; Ravichandran, K.; Pandiarajan,S.; Srinivasan.; Ravikumar, K.; Pushpa, C.P.; Swaminathan,K.; Arun, T. *Ceramics International.*, **2016**, 7336–7346.

7. Pandu, R. *Mat. Sci. Res.*, **2014**, 128-145.
8. Pooladi, M.; Shokrollahi, H.; Lavasani, S.A.N.H; Yang, H. *Materials Chemistry and Physics.*, **2019**, 39-48.
9. Hu, Z.T.; Liu, J.; Yan, X.; Oh, W.D; Lim, T.T. *Chemi. Engin. Journal.*, **2015**, 1022-1032.
10. Hussain, S.; Alam, M.M.; Imran, M.; Ali, M.A.; Ahamad, T.; Haidyrah, A.S.; Alotaibi, S.M.R.; Shariq, M. *Alexandria Engineering Journal.*, **2011**, 9107-9117.
11. Koo, P. L.; Choong, Z. Y.; Gasim, M. F.; Khoerunnisa, F.; Jaafar, N. F.; Saputra, E.; Oh, W. D. *Chemosphere.*, **2022**, 135619-135622.
12. Liu, Z.; Tan, Y.; Ruan, X.; Guo, J.; Li, W.; Li, J.; Ma, H.; Xiong, R.; Wei, J. "Int. J. Mol. Sci." . **2022**, 12652-12662.
13. Haidri, S.R.; Ahmad, F.; Javed, N. *Journal of Agricultural Sciences.*, **2021**, 1155-1159.
14. Vyas, V.G.; Kandoliya, U.K.; Vidhani, S.I.; Parmar, H.J.; Bhalani, V.M.; Golakiya, B.A.2015. *Int. J. Curr. Microbiol. App. Sci.*, **2015**, 839-843.
15. Zhang, S.; Xu, Z.; Ji, T.; Chen, Z.; Li, A.; Jv, D.; Guan, P.; Liang, T.; Ao, Z. *Surfaces and Interfaces.*, **2023**, 102809-102815.
16. Igara,C.E; Omoboyowa, D.A; Ahuchaogu, A.A; Orji, N.U. Ndukwe, M.K. *J. Pharmacogn. Phytochem.*, **2016**, 07-09.
17. Irshad, M.A.; Nawaz, R.; Ahmad, S.; Arshad, M.; Rizwan, M.; Ahmad, N.; Nizami, M.; Ahmed, T. *J. Environ. Sci. Manag.*, **2020**, 50–59.
18. Periasamy, A.P.;Yang, S.; Chen, S.M. *Talanta.*, **2011**, 2, 15-23.
19. Kumari, R.;Dwivedi, A.; Kumar, R.;Gundawar, M.K.; Rai, A.K. *Journal of Optics.*, **2022**, 1-16.
20. Nishan, M.; Subramanian, P. *J. Bio. & Env. Sci.*, **2014**, 27-35.
21. Chukwueze, G. N.; Asadu, C. O.; Onu, C. E.; Ike, I. S. *J. Eng. Res.*, **2020**, 6-17.
22. Gahlawat, D. K.; Jakhar, S.; Dahiya, P. *J. Pharmacogn. Phytochem.*, **2014**, 109-119.
23. Er, Ö.F.; Ula , B.; Kivrak, H.D. *Turkish Journal of Chemistry.*, **2021**, 1173-1188.
24. Manasa, G.; Bhakta, A.K.; Mekhalif, Z.; Mascarenhas, R. *J. Science for Energy Technologies.*, **2020**, 174-182.
25. Yıldız, C.; Bayraktepe, D.E.; Yazan, Z.; Önal, M., 2 *Journal of Electroanalytical Chemistry.*, **2022**, 116205-116213.
26. Zhang, X.; Fu, J.; Liu, Y.; Zhou, X.D.; Qiao, J. *ACS Sustainable Chemistry & Engineering.*, **2020**, 871-4876.
27. Maheshwaran, S.; Tamilagan, E.; Chen, S.M.; Akilarasan, M.; Huang, Y.F.; AlMasoud, N.; Abualnaja, K.M.; Ouladsmne, M.2021. *Microchimica Acta.*, **2021**, 1-11.
28. SA, F.S.A.; Al Marzouqi, F.; Ragamathunnisa, M.; AR, M. J.; Ayeshamariam, A. and Kaviyarasu, K., Synthesis and characterization of Bi_2O_3 NPS and photocatalytic application with methylene blue., **2021**.
29. Micheal, K.; Ayeshamariam, A.; Boddula, R.; Arunachalam, P.; AlSalhi, M.S.; Theerthagiri, J.; Prasad, S.; Madhavan, J.; Al-Mayouf, A.M. *Materials Science for Energy Technologies.*, **2019**, 104-111.
30. Kim, K.R.; Owens, G.; Kwon, S.I.; So, K.H.; Lee, D.B.; Ok, Y.S. *Water, Air, & Soil Pollution.*, **2011**, 163-174.
31. Saravanakkumar, D.; Abou Oualid, H.; Brahmi, Y.; Ayeshamariam, A.; Karunanaithy, M.; Saleem, A.M.; Kaviyarasu, K.; Sivaranjani, S.; Jayachandran, M. *OpenNano.*, **2019**, 100025-100030.
32. Mary, A.S.; Raghavan, V.S.; Kagula, S.; Krishnakumar, V.; Kannan, M.; Gorthi, S.S.; Rajaram, K. *ACS Appl. Bio Mater.*, **2021**, 8466–8476.